

Observability of fidelity decay at the Lyapunov rate in few-qubit quantum simulations

Max D. Porter and Ilon Joseph

Fusion Energy Sciences Program, Lawrence Livermore National Laboratory
October 13, 2021

In this work, the observation of the Lyapunov exponent in noisy quantum simulation experiments is shown to be bounded by three conditions that together make it presently out of reach. These conditions form a triangular region in parameter space with an area dependent on the number of qubits used. We predict that at least six qubits and $2.5 - 13\times$ less error per CNOT gate on IBM-Q or $0.87 - 9.6\times$ less error per Mølmer-Sørensen gate on IonQ are needed for the Lyapunov exponent to become experimentally observable. This prediction is achieved through close study of the quantum sawtooth map (QSM), which is the most efficiently simulated quantum system with a provably chaotic classical counterpart and rich dynamics.

1 Introduction

1.1 Motivation

Understanding chaotic dynamical systems is essential for understanding the world around us. Because chaotic systems are typically modeled through numerical computation, they are one of the primary application areas for scientific computing. Examples from classical physics include simulations of molecular dynamics, fluid dynamics, plasma physics, and gravitational N-body problems. Examples from quantum physics include non-equilibrium condensed matter physics, chemistry, nuclear physics, and lattice gauge theory. Since quantum computing offers a potential acceleration of many important calculations within scientific computing, chaotic dynamical systems stand to be one of the most important quantum computing application areas. In fact, because chaotic systems are provably difficult

Max D. Porter: porter42@llnl.gov

to simulate, recent claims of achieving quantum supremacy [1, 2] crucially rely on the exponential difficulty of simulating chaotic quantum circuits on a classical computer. Simulating quantum chaotic dynamics has even been proposed as the most qubit-efficient application for reaching useful quantum advantage [3].

Simulating *classical* chaotic systems on a quantum computer comes with a particular challenge: how can a nonlinear dynamical system be simulated in a linearly evolving quantum computer? Quantum computers were originally proposed [4, 5] because they are well-adapted to simulating quantum mechanical systems. A number of quantum algorithms for quantum Hamiltonian simulation have been proposed that can provide an exponential speedup over direct simulation [6]. Therefore a natural approach for classical Hamiltonian systems is to simulate their quantized versions. In fact, it was recognized early on that this technique can accelerate the computation of useful dynamical quantities, such as the Lyapunov exponents and classical diffusion coefficients of chaotic dynamical systems [7, 8]. This is possible even without using many qubits to approach the limit of classical dynamics.

Simulating non-Hamiltonian classical systems requires other approaches. Techniques for exactly simulating such systems have recently been proposed [9, 10, 11, 12, 13, 14]. The key is to embed the nonlinear system within an infinite-dimensional linear system, and then determine a finite-dimensional approximation that has sufficiently high accuracy for the purposes at hand. Then, if the linear system is unitary, as in the Koopman-von Neumann approach [9, 10], one can directly use Hamiltonian simulation algorithms. If it is not unitary, as in the Carleman linearization approach [11, 13], one can still use the quantum linear solver algorithm [15, 16] to propagate the state forward in time.

The speedup predicted for quantum simulation applies only to information that can be efficiently extracted. For dynamics this means collective properties like the Lyapunov exponent, localization length, and diffusion coefficient. The Lyapunov exponent is extracted from the fidelity of a quantum algorithm in the presence of noise. If the algorithm is exponentially efficient compared to classical methods, for instance by use of the quantum Fourier transform, the Lyapunov exponent inherits an exponential speedup [8]. The first big milestone then for the quantum simulation of classically chaotic dynamics is to observe the Lyapunov exponent on a noisy few-qubit quantum device. This milestone faces three limitations: the Lyapunov exponent must be less than the Fermi golden rule decay rate due to noise; the Lyapunov exponent must be large enough to avoid a phase transition to localization; and the noise must be small enough that sufficient time steps of the fidelity can be obtained. One must also consider the improvements in gate error rates that would be required to observe these effects on near term quantum computing hardware platforms. In order to establish a baseline for comparison, experiments on the open access IBM-Q superconducting platform and reported data for IonQ are considered for their relatively high qubit fidelities.

1.2 Quantum Maps

Classical maps are model systems of deterministic, often Hamiltonian, chaos and nonlinear dynamics, and their quantized counterparts are called quantum maps. Just as classical maps use discrete time steps to achieve rich dynamics at low computational cost, quantum maps are Floquet systems with trivial time ordering, leading again to discrete time steps and rich yet efficient dynamics. In the future, scalable, error-corrected devices will simulate quantum maps in their classical limit, resolving classical phase space structures larger than $\hbar/J_0 \sim 1/N$ for classical action J_0 and Hilbert space dimension N [7]. In the present and near term however quantum maps are an excellent tool for exploring the simulation of both quantum and classical chaos, while using minimal resources. Quantum maps have a numerically precise yet dense evolution operator and a simple classical correspondence principle. Coupled quantum maps are akin to spin chains

and allow the study of many-body physics without need for trotterization [17].

Specific algorithms using standard gate sets have been proposed for digital quantum simulations of quantized versions of the standard map [18], sawtooth map [7], kicked Harper map [19], tent map [20], and baker’s map [21].

The quantum baker’s map could be potentially interesting to study because it is the most efficient to implement, requiring only quantum Fourier transforms. However, one may need to generalize the form of the baker’s map in order to have enough free parameters to ensure the observability of the Lyapunov regime. This paper instead follows the work of Benenti et al. [7, 22, 23, 8] in using the second-most resource efficient quantum map, the quantum sawtooth map, which has been shown to have rich dynamics. It consists of four steps with $O(n^2)$ gates each, before accounting for topology or converting to gate depth. Theoretical studies looking at the quantum sawtooth map have often used ~ 10 qubits [8, 24], but this work seeks to find the smallest system size for which the Lyapunov exponent is still observable.

1.3 Loschmidt echo

Quantum maps have a long history as a tool for studying quantum chaos, quantum computing, and especially the Loschmidt echo (LE or “fidelity”). The nuanced relationship between these three has been outlined from various points of view in several review papers [25, 26, 27]. This fidelity typically measures the overlap of a state after time evolution under two different quantum Hamiltonians, one with and one without a perturbation. In order to match experiments, this work will use a “two-way” fidelity that is the overlap of two such evolutions that are independently perturbed. This overlap decays at a gradual and context-dependent rate in time, so it is useful also for linearized classical flows [28].

Asher Peres [29] initiated the study of how dynamics impacts fidelity decay in quantum systems and showed how this understanding can shed light on the classical-quantum correspondence principle for chaotic systems. This inspired a flurry of work decades later laying out regimes of quantum fidelity decay, most importantly for chaotic systems a Lyapunov exponent decay rate at large perturbations or weak chaos

[25, 30, 31]. This can be concealed by early time and late time decay regimes [25] and in certain cases by an oscillating decay rate at the transition to Lyapunov-rate decay [24, 32, 33]. Random matrix theory, semiclassical path integrals, and other methods have been employed to explain these regimes as well as more subtle effects [26, 25]. As applied to quantum computing, an important distinction is between static and random errors in the Hamiltonian, analogous at the gate level to coherent and incoherent errors in real quantum hardware [34]. Whereas random errors give exponential decay with linear dependence on the number of gates in the exponent, static errors can cause quadratic dependence for large numbers of gates [20]. In this work simulations only consider random error for simplicity, but static imperfections should be studied in the future.

Fidelity decay rates may serve as an especially useful signature of quantum chaos in quantum simulation. Where energy level statistics need many independent level spacings to resolve the distribution, fidelity decay relies on the more sensitive eigenstates. Eigenstate deformation was recently shown to be a more sensitive measure of quantum chaos than level statistics in a many-body system, and to be sensitive at increasingly small system sizes as the strength of perturbation grows [35]. This is somewhat supported by experiment: the level statistics approach was used to detect a quantum-chaotic to many-body-localized (MBL) transition in a nine-qubit specialized emulator [36], while recent work used the fidelity decay rate to detect a diffusive to localized transition in a three-qubit digital quantum simulator [37]. The fidelity is also a more accessible if coarser tool than measuring the energy spectrum and could simplify experiments.

1.4 Overview of Contents

In the next section, the sawtooth map is introduced in both classical (Sec. 2.1) and quantum (Sec. 2.2) form and its key properties are described. An expression is derived in Sec. 3.1 for the dynamical localization length in this system as well as a threshold for its observation. In Sec. 3.2 the system's noise-induced fidelity decay regimes are described, and related to previous work. In Sec. 4.1 formulas are derived for the three bounds restricting Lyapunov fidelity decay.

Then in Sec. 4.2 these parameter bounds are combined with numerical results, recent experiments, and reported fidelities to establish lower bounds for the necessary system size and reduction in noise relative to IBM-Q and IonQ's present day hardware in order to achieve a first observation of Lyapunov fidelity decay. Sec. 5 summarizes and provides some closing thoughts.

2 The Sawtooth Map

To begin, the classical and quantum sawtooth maps are defined, which are classically chaotic and quantum chaotic respectively. [38] This map is chosen for its efficient simulation of Hamiltonian chaos [37]. Expressions are given for the classical Lyapunov exponent and diffusion coefficient, which inform the analysis of the quantum dynamics.

2.1 Classical Sawtooth Map (CSM)

The classical sawtooth map (CSM) is governed by the periodically driven Hamiltonian

$$\tilde{H}_{CSM} = \frac{J^2}{2I} - \sum_n \tilde{K} \frac{\theta^2}{2} \delta(t - n\tau) \text{ for } \theta \bmod 2\pi \quad (1)$$

where (J, θ) are conjugate action-angle variables, τ is the driving period, I is a constant moment of inertia, and \tilde{K} is the kicking parameter with units of action. The sum n is over all integers. It is convenient to remove units from the equation, so the variables are transformed as $J = J'I/\tau$, $t = t'\tau$, $\tilde{K} = K'I/\tau$, $H = H'I/\tau^2$ then the primes are dropped to get

$$H_{CSM} = \frac{J^2}{2} - \sum_n K \frac{\theta^2}{2} \delta(t - n) \text{ for } \theta \bmod 2\pi \quad (2)$$

with dimensionless kicking parameter K . Integrating Hamilton's equations of motion over one period gives the map

$$\begin{aligned} J_{n+1} &= J_n + K\theta_n \bmod 2\pi L \quad (-\pi L \leq J < \pi L) \\ \theta_{n+1} &= \theta_n + J_{n+1} \bmod 2\pi \quad (-\pi \leq \theta < \pi) \end{aligned} \quad (3)$$

where L is a positive integer to ensure no discontinuous behavior in the second (free evolution) equation. In the limit $L \rightarrow \infty$ the map's manifold shifts from a torus to a cylinder. The non-linearity of the map arises from its modulo operation. While its dynamics are fully regular for

$-4 < K < 0$, they become chaotic for $K > 0$ and $K < -4$. The maximal Lyapunov exponent describing the strength of the chaos is

$$\lambda(K) = \ln[(2 + K + \text{sgn}(K)\sqrt{K^2 + 4K})/2] \approx \begin{cases} \ln[K + 2 + O(K^{-1})] & \text{for } K \gg 1 \\ K^{1/2} - \frac{1}{24}K^{3/2} + \frac{1}{4}K^2 - O(K^{5/2}) & \text{for } 0 < K \ll 1 \end{cases} \quad (4)$$

[8]. For this paper we choose to restrict the analysis to $K > 0$.

Diffusion in classical chaotic systems can be understood as that of a random walk in the action J , where the probability density function obeys the Fokker-Planck equation. The main result is that the CSM diffusion coefficient is

$$D_K \approx \begin{cases} (\pi^2/3)K^2 & \text{for } K > 1 \\ 3.3K^{5/2} & \text{for } 0 < K < 1 \end{cases} \quad (5)$$

where the first case comes from a random phase approximation, and in the latter case trajectories stick to broken cantori which slows diffusion [8].

2.2 Quantum Sawtooth Map (QSM)

The quantum sawtooth map (QSM) can be straightforwardly derived from the classical Hamiltonian of Eq. 2. The action variable J is quantized by enforcing the canonical commutation relation $[\hat{\theta}, \hat{J}] = i\hbar$, where \hbar is the dimensionless Planck's constant given by $\hbar_{phys} = \hbar'I/\tau$ then dropping the prime. For computability θ is then discretized in a computational basis. This limits J to a finite number of values, as the size of the two bases must be equal for transformations between them to be possible. The operator eigenvalues are then

$$\begin{aligned} \hat{J}|p\rangle &= \hbar p|p\rangle; \quad p = -N/2, \dots, (N-1)/2 \\ \hat{\theta}|q\rangle &= 2\pi q/N|q\rangle; \quad q = -N/2, \dots, (N-1)/2 \end{aligned} \quad (6)$$

where N is the chosen basis size, which in the context of quantum computing is naturally chosen to be $N = 2^n$ for n qubits. States $|q\rangle$ and $|p\rangle$ will be referred to as the canonical position and momentum eigenstates respectively.

The quantized Hamiltonian results in a quantum evolution propagator over each period given

by

$$\begin{aligned} U_{QSM} &= \hat{T} \exp\left(-i \int_0^1 H_{QSM} dt / \hbar\right) \\ &= U_{kin} U_{pot} \\ U_{pot} &= \exp\left(ik(\beta\hat{q})^2/2\right) \\ U_{kin} &= \exp\left(-i\hbar\hat{p}^2/2\right) \end{aligned} \quad (7)$$

where \hat{T} is the time-ordering operator, $k \equiv K/\hbar$ is the quantum kicking parameter, and $\beta \equiv 2\pi/N$ for N basis states. This single-period propagator is often called a Floquet operator, but since it corresponds to a classical map it is also referred to as a quantum map. Quantum map propagators are particularly simple to calculate as the delta-function in the potential makes time ordering trivial. The eigenstates of the quantum map are also eigenstates of the so-called Floquet Hamiltonian, the matrix logarithm of the time-averaged evolution operator, so one can refer to them as Floquet eigenstates or quasienergy eigenstates. Their phase evolution controls the evolution of the system.

In the quantum map the classical kicking parameter K has split into $k = K/\hbar$ and \hbar . Matching the periodicities of the classical and quantum systems further requires $\Delta J = 2\pi LM = \hbar N$, where L and M are positive integers and $M = 1$ is set without loss of generality. This restricts Planck's constant to $\hbar = 2\pi L/N$. The classical limit of the QSM is achievable only in the many-qubit limit $N \rightarrow \infty$, causing $\hbar \rightarrow 0$ and $k \rightarrow \infty$ while keeping the classical parameter $K = k\hbar$ constant. In this study $L = 1$ is chosen to maximize the chance of observing a Lyapunov decay rate, based on the bounds in Sec. 4. Then K is varied (controlling $\lambda(K)$) and noise amplitude σ (see Sec. 3.2) to explore the dynamics. A range of system sizes relevant to present day and near term quantum devices are considered, $3 \leq n \leq 12$. Note that making L even would allow L/N to simplify and reduce the pseudorandomness of the phase operators, disrupting the chaotic dynamics.

3 Dynamics

3.1 Dynamical Localization

In the field of quantum chaos, quantum analogs of classically chaotic systems are well-known to

diffuse classically until reaching a steady state exponential localization of the wave function

$$P_p = |\langle p|\psi\rangle|^2 \approx \frac{1}{\ell} \exp\left(-\frac{2|p-p_0|}{\ell}\right), \quad (8)$$

for initial momentum $|p_0\rangle$, under certain conditions. The localization length ℓ is reached after the Heisenberg time $\tau_H \approx \ell$ [8]. The heuristic explanation is that initially there is classical diffusion of strength D_K , but this transitions at the Heisenberg time to coherent oscillations of frequencies $\omega = \Delta E/\hbar$ between (quasi)energy eigenstate pairs with energy differences ΔE . The Heisenberg time is when these oscillations dominate, $\tau_H = 2\pi\hbar/\Delta E_{\text{ave}}$ [39]. The randomness of these pair oscillations causes a net effect of localization around the initial state. The balance of these processes is captured by the approximation

$$\begin{aligned} \ell &\approx D_K/\hbar^2 \\ &\approx \begin{cases} (\pi^2/3)k^2 & \text{for } K > 1 \\ 3.3k^{5/2}(2\pi L/N)^{1/2} & \text{for } 0 < K < 1 \end{cases} \end{aligned} \quad (9)$$

using Eq. 5 and $K = k * 2\pi L/N$ [8, 23]. In practice dynamical localization is reflected in localized Floquet eigenstates, with the Floquet evolution only including Floquet eigenstates in proportion to their overlap with the initial condition. For $0 < K < 1$ there may also occur a second localization regime with slower scaling in k as seen in other quantum maps [40, 41, 42]. This has not been studied for the quantum sawtooth map, but would be in the strongly localized regime and unlikely to affect the border to diffusion below.

Using the expressions for ℓ and for the localized distribution, the condition for observing any localization should be that P_p has decayed by less than $1/2$ at the edge, or else the overlap of the tails would cause full diffusion. This gives the condition

$$\begin{aligned} 1/2 &> \exp(-N/\ell) \\ \ell &< N/\ln(2) \\ k &< k_{\text{loc}} \\ &\equiv \begin{cases} \sqrt{\frac{3}{\ln(2)\pi^2}}N \approx 0.66N^{1/2} & \text{for } K > 1 \\ \left(\frac{1}{3.3\sqrt{2\pi\ln(2)}}\frac{N^{3/2}}{L^{1/2}}\right)^{2/5} \approx 0.50N^{3/5}L^{-1/5} & \text{for } 0 < K < 1 \end{cases} \end{aligned} \quad (10)$$

for localization, alternately written as

$$K < K_{\text{loc}} \approx \begin{cases} 4.16LN^{-1/2} & \text{for } K > 1 \\ 3.12L^{4/5}N^{-2/5} & \text{for } 0 < K < 1. \end{cases} \quad (11)$$

Note that the QSM becomes a quantum cat map when $K/L \in \mathbb{Z}$ ($2\pi k/N \in \mathbb{Z}$). In such cases the generic behaviors of localization and diffusion are replaced by periodic behavior with regular structures in phase space. Cat maps arise when the potential energies $\arg(U_{\text{pot}}) = K/L * \beta q^2/2 \bmod 2\pi$ are not pseudorandom over q . However even small perturbations can restore the generic QSM behavior, so the large noise considered in this paper make cat maps' periodic behavior difficult to observe in practice [38].

3.2 Noise

3.2.1 Noise Model and Fidelity

For this paper a simple parameter noise model is used, where the quantum kicking strength k is perturbed at each step by $k \rightarrow k + \zeta$. The noise is random and drawn from a normal distribution with standard deviation σ , where the PDF is given by

$$p(\zeta) = \frac{1}{\sqrt{2\pi}\sigma} \exp\left(-\frac{\zeta^2}{2\sigma^2}\right). \quad (12)$$

This noise model easily extends to the classical map by perturbing the classical kick $K = k\hbar$ with standard deviation $\epsilon = \sigma\hbar$. Quantum noise can also be controlled by K by keeping \hbar constant as will be done here.

Below, the effect of noise on the rate of fidelity decay of the quantum system is studied. The fidelity of a noisy unitary evolution U_σ can be measured by

$$f(t) = |\langle \psi | U_\sigma^{-t} U_\sigma^t | \psi \rangle|^2 \quad (13)$$

which is also known as the Loschmidt echo. In words, an initial state $|\psi\rangle$ is evolved for a discrete number of time steps t by a unitary process U_σ formed from an ideal U and a noisy process of magnitude σ . The inverse operation is then attempted in order to recover the original state, with the fidelity of success $f(t)$ measured in the basis of the initial state. (For non-unitary, Markovian noise processes the above would require a Lindblad master equation instead.) Contrary to previous studies, “two-way” noise is used

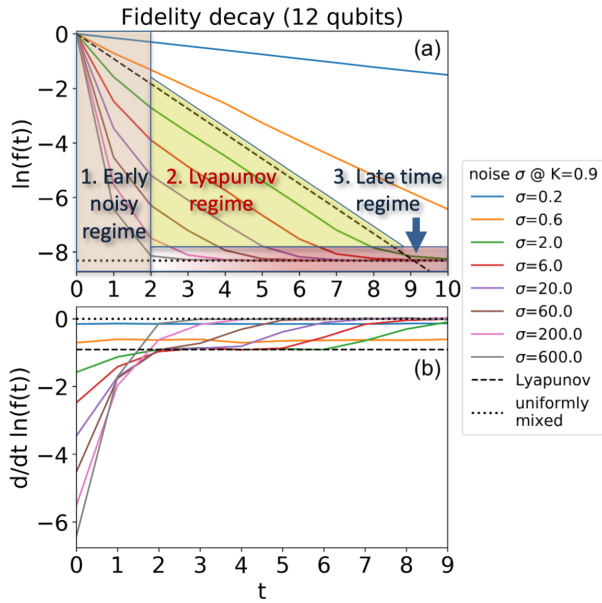


Figure 1: (a) Simulated fidelity decay $f(t)$ and (b) exponential rate of fidelity decay $-\gamma(t) \equiv d/\ln(f(t)) = \ln(f(t+1)) - \ln(f(t))$ as noise σ is varied. Parameters $n = 12, K = 0.9, L = 1$ for diffusive dynamics. Dashed lines show the classical Lyapunov decay $\exp(-\lambda t)$ and dotted lines show the uniformly mixed limit $1/N$.

that affects both forward and backward evolution, to keep closer to experiment where noise cannot be turned off. This increases the fidelity decay rate at given σ by a factor of two.

3.2.2 Quantum Effects of Noise

In Fig. 1 a python simulation of the QSM is implemented with random parameter noise. Over a range of noise magnitude σ there emerge three time regimes: a fast early time decay, a slower intermediate time decay, and an even slower late time decay. The intermediate time regime either corresponds to the Fermi golden rule decay rate for sufficiently weak noise or to the Lyapunov decay rate for sufficiently strong noise.

The early and intermediate time regimes can be understood from a simple model. Derived in [30] but clarified in [31, 43, 44] is the chaotic fidelity decay rate

$$f(t) = \bar{A} \exp(-\lambda t) + B \exp(-\Gamma t) + 1/N \quad (14)$$

for Fermi golden rule decay Γ , classical Lyapunov exponent λ , parameter-dependent coefficient \bar{A} , and constant B . At intermediate time this translates to $f(t) \propto \exp(-\min(\lambda, \Gamma)t)$ as the faster decay quickly depletes itself and leaves the slower

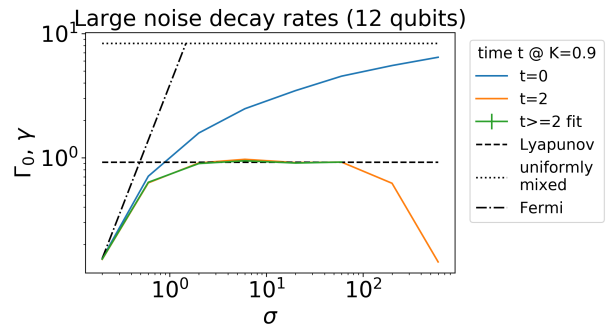


Figure 2: Simulated fidelity decay rates as functions of noise σ : initial decay rate $\Gamma_0 = -(\ln(f(1)) - \ln(f(0)))$ and intermediate time decay rate $\gamma = \min(\lambda, \Gamma)$ measured at $t = 2$ and measured by an exponential fit of the intermediate time regime. Same parameters as Fig. 1. Fermi golden rule decay $C\sigma^2$ projected using C from the smallest σ .

decay to dominate. However at early times \bar{A} diverges and the first term's derivation is invalid, leaving only golden rule decay. The distinction between early time and intermediate time regimes is most distinct in Fig. 1(b) which shows the decay rate at large (but not too large) noise beginning faster than the Lyapunov rate, reducing to the Lyapunov rate for several steps, and finally dropping to zero during late time decay.

Late time decay slows as it asymptotically approaches the uniformly mixed limit $1/N$. The slowing can be removed by assuming the form

$$f(t) = f'(t)(N-1)/N + 1/N \quad (15)$$

and “unfolding” the intermediate time trend as $f'(t) = N/(N-1) * (f(t) - 1/N)$. This may restore useful data points of Lyapunov decay that would otherwise be lost, as shown in Fig. 5

In Fig. 2 the early and intermediate time decay rates are shown as functions of the noise over orders of magnitude. Initial decay rate Γ_0 is measured as the decay rate at $t = 0$, while intermediate time decay rate γ is measured both as the rate at $t = 2$ and from fitting (γ, t_0) to the form $f(t) = \exp(-\gamma(t - t_0))$ for only points in the intermediate time regime, where $t \geq 2$ and $f > 2/N$. The two methods agree, except at large noise where the intermediate time regime includes less than two data points so the fit becomes underconstrained. Initial decay is seen to quickly diverge from the Fermi golden rule, which predicts $\Gamma_0 = C\sigma^2$ for noise σ and some constant C . Instead it asymptotically approaches the uniformly mixed limit of reaching $f(1) = 1/N$ after

a single step. This slowing relative to golden rule decay is crucial to observing the Lyapunov rate on small systems. Intermediate time decay follows $\gamma = \min(\lambda, \Gamma)$ until sufficiently large noise destroys this regime.

It should be noted that the early time regime of the QSM described here has not been observed in other models or analyses [25], though it appears to be discernible in the QSM in Ref. [8]. Perturbation theory predicts a Gaussian early time decay instead [25], but for this map discrete time steps and fast decay cannot resolve its very short time scale. The nearly constant duration $t_{\text{early}} \approx 2$ of this early time regime does not match predictions either. Ref. [44] provides $t \geq 1/\Gamma$ as the minimal time before Lyapunov decay appears, yet for $1 \leq \Gamma \leq 4$ considered in Fig. 1 that would predict one discrete time step rather than the observed two.

Lastly, we were unable to observe the bandwidth limit mentioned in Ref. [25] after a search up to 14 qubits. This is assuming a bandwidth B_{QSM} no greater than the 2π given for the kicked rotator in the same reference. The bandwidth limit is the maximum fidelity decay rate that is reached when the perturbed Floquet eigenstates have maximally spread across the unperturbed Floquet eigenstates, as measured by the local spectral density of states. Further study may find whether this lack of a bandwidth limit is due to the initial conditions, system choice, or otherwise. Regardless it is convenient for exploring other dynamics to not have such a restriction.

4 Lyapunov rate decay

An important goal for the simulation of chaotic systems on few-qubit and NISQ devices is the experimental observation of the Lyapunov exponent. A simple method for observing the classical Lyapunov exponent in a strongly quantum system is through its fidelity decay rate, as described in Sec. 3.2.2. (Or through related quantities like out-of-time-ordered correlators (OTOCs) discussed in Sec. 5.) Here are described three limitations to observing the Lyapunov exponent in the fidelity decay rate in any chaotic quantum system, with quantitative bounds given from those limitations for the QSM.

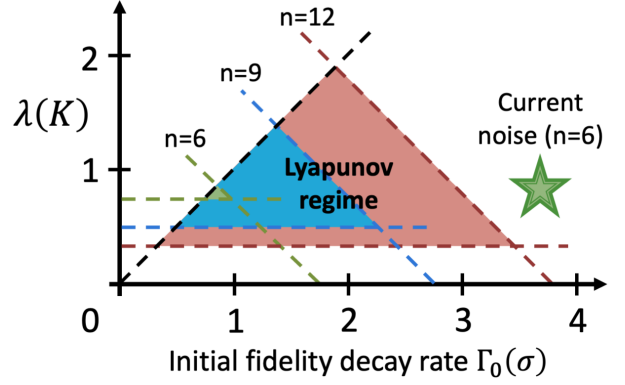


Figure 3: Parameter space showing when the Lyapunov exponent can be observed in the fidelity decay of the noisy QSM. Axes are the initial fidelity decay rate $\Gamma_0(\sigma) = -(\ln(f(1)) - \ln(f(0)))$, dependent on noise magnitude σ at given n , and the classical Lyapunov exponent $\lambda(K)$. Dotted lines show bounds, with solid color regions indicating when Lyapunov decay is clearly observable at different qubit numbers n .

4.1 Three bounds

The first limitation is that intermediate time fidelity decay of a classically-chaotic quantum system goes as $f(t) \propto \exp(-t \min(\lambda, \Gamma))$ for classical Lyapunov exponent λ and Fermi golden rule decay rate Γ . This has been well established since the first papers on Lyapunov quantum fidelity decay [31, 25] and is shown in the QSM in Sec. 3.2.2. The condition for observing the Lyapunov rate is then **bound (1)**:

$$\Gamma(\sigma) > \lambda(K). \quad (16)$$

The initial golden rule decay rate Γ_0 and intermediate time golden rule decay rate Γ are typically equal (see Fig. 1(a) for small σ) so it is assumed that $\Gamma = \Gamma_0$ when drawing this bound in Fig. 3.

The second limitation is due to dynamical localization, discussed in Sec. 3.1. In the weak chaos limit of small k (implying small K and λ for constant L), the localization puts a halt to chaotic diffusion. Level statistics show that as localization length $\ell \rightarrow 0$ the dynamics transition gradually from quantum chaotic to entirely regular [45]. This causes a transition from exponential to algebraic fidelity decay [25]. Simulations of the QSM with a simple noise model show this transition on at least five qubits, though experimentally the transition has been observed on three qubits [37].

One can obtain a diffusion bound specific to when Lyapunov decay is desired by using small

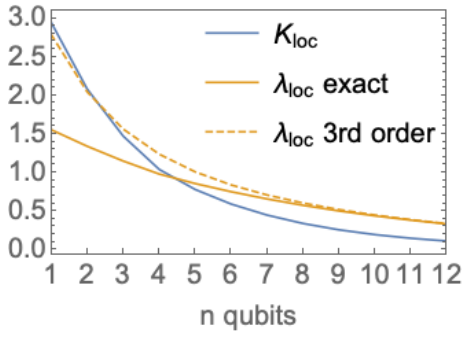


Figure 4: Parameter values below which localization occurs in the QSM, from Eq. 11, Eq. 4, and third order of Eq. 17, respectively.

L and large N , which increase the chance of diffusion and therefore Lyapunov decay. From Eq. 11 these limits enter the $0 < K_{\text{loc}} < 1$ cantori regime, meaning diffusion occurs when $K > K_{\text{loc}} \approx 3.12L^{4/5}N^{-2/5}$. Assuming $N \gg 17.3L^2$ implies that $0 < K_{\text{loc}} \ll 1$, allowing use of the power expansion of $\lambda_{\text{loc}}(K_{\text{loc}})$ in Eq. 4 to derive **bound (2)**:

$$\lambda(K) \gtrsim 1.77 \frac{L^{2/5}}{N^{1/5}} - 0.23 \frac{L^{6/5}}{N^{3/5}} + 2.43 \frac{L^{8/5}}{N^{4/5}} + \dots \quad (17)$$

This bound is approximate for several reasons. First, the diffusion bound is heuristically derived and imprecise. Second, since localization occurs after about ℓ time steps and ℓ is large near the bound, Lyapunov decay could still occur during the initial classical diffusion, suggesting this bound is too strict. However in practice distinguishing the transition to localization may be difficult in few-qubit experiments. The algebraic decay due to localization appears to pass through many “exponential” rates and may be mistaken for a single step of exponential Lyapunov decay during the initial classical diffusion. This suggests two steps of Lyapunov decay are needed, similar to Figs. 1 with $\sigma = 20$, which will be accounted for in the bound (3). Third and lastly, it was assumed that $n = \log_2(N) \gg 4$ (when $L = 1$). For the small n of current experiments one should instead calculate K_{loc} from Eq. 11 and plug into the exact $\lambda(K)$ of Eq. 4 directly. This approach is compared to the third order expansion in Fig. 4.

The third limitation is competition from the early time and late time decays. Sufficient noise leading to short decay can cause the intermediate time Lyapunov decay to get squeezed out.

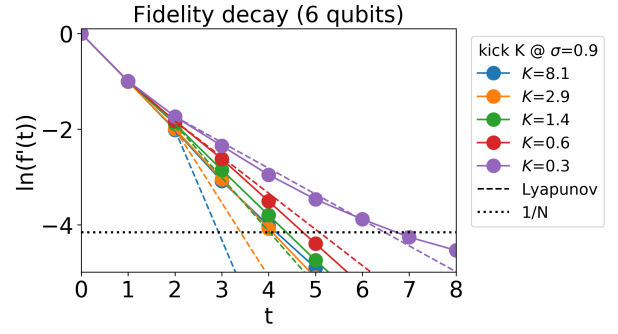


Figure 5: Simulations of minimal-qubit Lyapunov decay, where $n = 6, \sigma = 0.9, L = 1$ and K is varied. Dashed lines show theoretical Lyapunov decay projected from a start at $t_{\text{early}} = 2$. Comparing the golden rule decay for $K \geq 2.9$ to Lyapunov decay at $K = 0.6$ shows a small but noticeable difference. Localization-slowed decay at $K = 0.3$ has a subexponential trend that is difficult to clearly distinguish from Lyapunov decay at intermediate times. Localization occurs for $K < K_{\text{loc}} = 0.59$.

Figs. 1 and 2 demonstrate this at large noise where the Lyapunov rate is no longer visible. Since early time decay is numerically observed to end at $t = t_{\text{early}} \approx 2$ fairly consistently and late time decay is seen to begin at $f = a_{\text{late}}/N$ with $a_{\text{late}} \approx 2$, one can write a bound on the initial decay rate Γ_0 to ensure these two don’t meet as $\exp(-\Gamma_0 t_{\text{early}}) \gtrsim a_{\text{late}}/N$. A stricter bound requiring a clear Lyapunov signature must include a number of intermediate time steps t_{lyap} at the Lyapunov rate, to avoid the ambiguity with algebraic decay. We choose $t_{\text{lyap}} = 2$ as a reasonable minimal number of Lyapunov steps. This gives $\exp(-\Gamma_0 t_{\text{early}} - t_{\text{lyap}} \lambda) \gtrsim a_{\text{late}}/N$ or **bound (3)**:

$$\Gamma_0(\sigma) \lesssim (\ln(N/a_{\text{late}}) - t_{\text{lyap}} \lambda(K))/t_{\text{early}}. \quad (18)$$

Unfolding the late time regime may be helpful here by reducing a_{late} . Since Γ_0 varies with σ more slowly than the quadratic Fermi golden rule prediction, as shown in Fig. 2, so Eq. 18 can be satisfied at surprisingly large noise σ .

These three bounds taken together form a triangular “Lyapunov regime” in parameter space as shown in Fig. 3.

4.2 Qubit and noise requirements

To show how a search for Lyapunov-limited decay may look in practice, a demonstration with a simple noise model on six qubits is provided in Fig. 5. In an experiment the noise cannot be easily varied, except to artificially increase it, but K can

be varied freely. For a noise magnitude within the appropriate triangle in Fig. 3, reducing K within the triangle reduces the decay rate to the Lyapunov rate $\lambda(K)$ for times $t > t_{\text{early}} \approx 2$, but only until localization begins at K_{loc} at the triangle's bottom. For six qubits the allowed range of noise and K are both minuscule, so the effect is very subtle and lasts closer to one time step than two. This is despite unfolding the late time behavior per Sec. 3.2, which should slightly increase the number of Lyapunov steps observed. Still, the numerical results conform well to the theoretical prediction that six qubits is the minimal system size at which a Lyapunov decay rate may barely be observed.

Since present day quantum computers have far surpassed six qubits in size and are limited primarily by noise, it is important to also determine the noise reduction needed to reach the triangular Lyapunov regime in Fig. 3. One can start with a baseline from the recent experiments on IBM-Q in Ref. [37]. First, for $n \geq 4$ a single QSM time step forward and back has negligible fidelity ($\sim 1/N$), implying a Γ_0 far outside of bound (3). At $n = 3$ fidelity is non-negligible and Γ_0 can be calculated using $\exp(-\Gamma_0) = f(1)$. Note that in the localization regime $\Gamma_0(\sigma)$ is found to also depend on K , yet since diffusive values of K are the focus this can be neglected. For diffusive $k = 2.0 \Rightarrow K \approx 1.6$ a fidelity of $f(1) \approx 0.25$ is observed, giving $\Gamma_0 \approx 1.4$. This is much greater than the predicted bound (3) for $N = 8$ and $\lambda(K) \approx 1.2$, which gives a nonsensical value of $\Gamma_{0,\text{crit}} = -0.49$. For three qubits then satisfying even just bounds (2) and (3) appears impossible.

From this baseline $\Gamma_0 \approx 1.4$ on three qubits, one can attempt to extrapolate to a desired Γ_0 on six qubits and predict how much current IBM-Q hardware must improve to reach the Lyapunov regime. A useful way to ask this is: By what factor does infidelity per CNOT gate ϵ need to be reduced? To answer this one can first connect Γ_0 to ϵ . To do so, combine two expressions for total one-step fidelity, $f(1) = \exp(-\Gamma_0)$ and $f(1) = (1 - \epsilon)^G$, for gate depth G of CNOT gates. This produces

$$\begin{aligned} \epsilon(n) &= 1 - \exp(-\Gamma_0/G(n)) \\ &\approx \Gamma_0/G(n) \quad \text{for } G(n) \gg \Gamma_0 \end{aligned} \quad (19)$$

where G for the given algorithm has some scaling with number of qubits n , and average ϵ of a qubit

cluster empirically increases with n . Applied to the three-qubit case, this implies $\epsilon(3) \approx 1.4/29 \approx 0.048$. Note this is $\sim 5\times$ larger than the $\epsilon(3) < 0.01$ reported by IBM-Q. This discrepancy may potentially be due to crosstalk, which IBM-Q's reporting neglects, as will be discussed shortly.

Eq. 19 can be used to extrapolate from a known case ($n = 3$, diffusive) to an unknown case ($n = 6$, Lyapunov regime) by determining three factors. They are the three reductions in CNOT error ϵ required to: reduce initial decay rate Γ_0 to a value in the six-qubit Lyapunov regime per Fig. 3; offset the increased gate depth $G(n)$ of larger algorithms; and offset the increased $\epsilon(n)$ due to crosstalk in larger qubit clusters. Then the factor by which current IBM-Q hardware error needs to be reduced to observe the Lyapunov regime will be $r \equiv a_{\text{decay}} * b_{\text{depth}} * c_{\text{crosstalk}}$, naming the three reduction factors respectively.

For a_{decay} , the goal is to move from the observed $\Gamma_0 \approx 1.4$ to the $\Gamma_0 \approx 0.9$ that will be needed for six qubits according to Fig. 3. The corresponding increase in $\epsilon(n)$, for any $n \geq 3$, would be $a_{\text{decay}} \approx 1.4/0.9 \approx 1.6$.

Calculating b_{depth} requires an estimate of the QSM algorithmic scaling of gate depth $G(n)$ with n on IBM-Q. In Ref. [37] the worst-case scaling is found to be $O(n^3)$, implying that $b_{\text{depth}} = (6/3)^3 = 8$. This worst-case scenario assumes linear qubit topology for minimal connectivity, a lack of effective gate optimization algorithms that could reduce the cost of poor qubit connectivity, and a lack of parallelization of CNOT gates such that their gate depth is nearly equal to their gate count. On IBM-Q nearly linear topology and minimal connectivity for six physical qubits is true on all of their current devices. All-to-all connectivity in superconducting architectures has been explored by multiple groups [46, 47], which would reduce gate depth scaling to at worst $O(n^2)$ [37]. However IBM-Q's gate optimization algorithms may already provide some fraction of that improvement. (Other architectures, such as many ion traps, already have all-to-all connectivity, even despite linear topology.) Some parallelization of CNOT gates also seems likely on IBM-Q, with the limit of a fully parallelized and fully connected gate depth scaling of $O(n)$ [37]. For a best-case scenario one can compare the gate depths of linear, non-parallelizable $n = 3$ and a fully-connected, fully-parallelized

$n = 6$. This involves several factors: first, fully connecting $n = 3$ reduces gate count and depth by $29/17 \approx 1.7$ [37]; then scaling up to $n = 6$ with full connectivity but no parallelization increases gate count and depth by $(6/3)^2 = 4$; lastly, full parallelization reduces gate depth by $n/2 = 6/2 = 3$. Altogether this suggests a $4/(1.7 * 3) \approx 0.78$ *smaller* gate depth! The reduction of ϵ needed on IBM-Q then varies from $b_{\text{depth}} = 8$ in the worst case to $b_{\text{depth}} \approx 0.78$ (an increase in ϵ) in the best case, spanning an order of magnitude.

The last factor $c_{\text{crosstalk}}$ measures the main expected increase in error per gate for larger qubit clusters: crosstalk error, where a gate acts on more qubits than was intended. This process is not captured by IBM-Q’s reported gate errors, which are measured with randomized benchmarking on the target qubits only [48]. The specifics of crosstalk can vary greatly between different architectures, such as between superconducting and trapped ion systems or between different implementations within each qubit type. It is common however for crosstalk to primarily affect “neighbor” qubits, those nearest to the target qubits in configuration space as well as frequency space. To a first approximation on IBM-Q, the scaling of crosstalk errors should depend on the average number of spatial neighbors for a two-qubit gate as the system size increases. However crosstalk occurs not only with the other qubits involved in the simulation, but also with nominally uninvolved neighbor qubits. Since crosstalk goes both ways, changing the intended evolution for both the target and off-target qubits, this crosstalk with nominally uninvolved qubits still causes relevant error. This implies $O(1)$ scaling of crosstalk with n within a given topology, since number of crosstalk neighbors per gate does not depend on how many neighbors are involved in the simulation. However this still implies a strong dependence on topology. For the worst-case scenario we assume linear topology, which should have an average of two neighbors per two-qubit gate, independent of n , neglecting the chain ends. For the best-case scenario we assume all-to-all connectivity, which should have $(n_{\text{chip}} - 2)$ neighbors per two-qubit gate for n_{chip} qubits on the physical chip. We don’t know how large n_{chip} might be in this hypothetical chip so we generously assume $n_{\text{chip}} = 6$

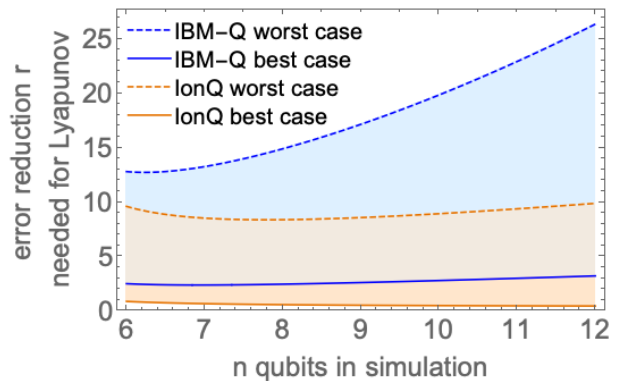


Figure 6: The factor by which error per two-qubit gate must be reduced on IBM-Q and lonQ for them to reach the Lyapunov regime, as a function of number of qubits n used in the simulation. For each two possible future cases are considered: the best case assumes all-to-all connectivity and maximal parallelization, while the worst case makes the fewest such assumptions based on current hardware. For IBM-Q recent relevant experiments are used, while for lonQ a benchmarking paper is used.

for $n = 6$. Then $c_{\text{crosstalk}}$ in scaling from the current $n = 3$ to a hypothetical $n = 6$ spans from $c_{\text{crosstalk}} = 1$ in the worst-connectivity case to $c_{\text{crosstalk}} = (6 - 2)/2 = 2$ in the best. However this factor has the most contextual uncertainty and should be tailored to the hardware of any specific experiment.

Combining these results produces an estimate for the factor reduction in error per IBM-Q CNOT gate needed to reach the Lyapunov regime on six qubits. By considering the best- and worst-case scenarios, one finds a reduction factor of $r = a_{\text{decay}} * b_{\text{depth}} * c_{\text{crosstalk}} \in [2.5, 13]$, with most of the variance depending on qubit connectivity and how well CNOT gates parallelize in the six-qubit QSM, which itself varies with connectivity. At large n the best case scales as $r \sim n$ while the worst case scales as $r \sim n^2$, both having a small coefficient.

This analysis can be extended to more than six qubits, as shown in Fig. 6. First a_{decay} decreases as the Lyapunov regime expands in size. It can be defined as the required change in Γ_0 to reach the intersection of bounds (2) and (3) at the rightmost corner of Fig. 3. With our observed bound

(3) parameters this means

$$\begin{aligned} 1/a_{\text{decay}} \propto \Gamma_0^{\text{max}} \approx \ln(N/2)/2 - 1.77 \frac{L^{2/5}}{N^{1/5}} \\ + 0.23 \frac{L^{6/5}}{N^{3/5}} - 2.43 \frac{L^{8/5}}{N^{4/5}}. \end{aligned} \quad (20)$$

using third order in λ_{loc} as a decent approximation at $n \geq 6$ according to Fig. 4. The ratio between Γ_0 at $n = 6$ and a larger $n > 6$ can be multiplied by $a_{\text{decay}}(n = 6) \approx 1.6$ to get $a_{\text{decay}}(n > 6)$, which should get smaller as n and Γ_0 get larger. The scaling of b_{depth} is between $O(n)$ and $O(n^3)$, so again those scalings relative to the best and worst minimum cases $b_{\text{depth}}(n = 6) \approx [0.78, 8]$ give $b_{\text{depth}}(n > 6)$. Lastly $c_{\text{crosstalk}}(n > 6)$ is respectively $(n - 2)/4$ (fully connected) to 1 (linear topology) times larger than $c_{\text{crosstalk}}(n = 6) = [2, 1]$ in the best and worst overall cases. These combine to give a wide range of possible r , depending on the connectivity and parallelizability of future devices. The prospect of observing the Lyapunov regime on 12 qubits is not as dismal as one might expect. In the best case scenario of good connectivity and parallelization, the added difficulty of having more noise per time step is largely canceled by the extended Hilbert space, since a smaller $1/N$ limit allows a longer fidelity decay in which to observe the Lyapunov regime. This means many-qubit ($n > 12$) Lyapunov simulations could become achievable at the same time as six-qubit simulations. An even lower estimate of r is also possible if efficient gate scaling and minimal crosstalk scaling are simultaneously achieved, which was not considered here. Lastly, to clarify, r is the factor by which the sum of all known or unknown sources of error should, as a whole, be reduced, as measured experimentally within a chaotic algorithm on several qubits, in order to reach the Lyapunov regime. Reducing the effects of crosstalk could be one way to achieve this change, but reducing gate times and environmental noise would help as well. This estimate of r does not claim to capture every aspect of scaling up, but hopefully captures the main considerations for today's leading devices.

Ion traps are another major architecture type, and it is worth estimating how far they might be from the Lyapunov regime. A single CNOT gate from the QSM decomposition can be converted to a single Mølmer-Sørensen gate plus

single-qubit gates [49], so the same scaling of two-qubit gates applies. IonQ is chosen here to represent current capability since they have demonstrated algorithms on an 11-qubit quantum computer [50], making them competitive with IBM-Q. They benefit from already having all-to-all connectivity and linear topology, though they do not offer parallel gates. (Limited parallel gates have been shown possible on IonQ, but not yet useful [51]. The QCCD architecture employed by Honeywell and others is however suited for full parallelization. [52])

IonQ's reported average error per two-qubit gate is 0.025, measured by preparing a bell state. This is worse than IBM-Q's reported error of < 0.01 , but neither fully account for crosstalk. On IBM-Q the error per gate during the QSM was 5x worse than the reported error, so without running the QSM on IonQ it is unclear how much worse it will be. IonQ do run algorithms, though less dynamically complex than the QSM, and find their Hidden Shift algorithm drops from a predicted average fidelity $f = 0.55$ to an observed $f = 0.35$ when using 10 two-qubit gates. They attribute this to crosstalk, which can be modeled as larger average error per two-qubit gate. The measured error can then be calculated from $0.55/0.35 \approx ((1 - 0.025)/(1 - \epsilon))^{10}$ which gives $\epsilon \approx 0.068$, a 2.7x worse error than reported. Since this algorithm is less dynamically complex than the QSM, this is compatible with measured error for the QSM being as much as 5x worse than reported, as it was for IBM. Consider these the best and worst cases, giving a range of a_{decay} . For the QSM using $G(3) = 17$ for all-to-all connectivity [37], one finds $\Gamma_0 \in 17 * [0.068, 0.13] \approx [1.2, 2.2]$ and so $a_{\text{decay}} \in [1.2, 2.2]/0.9 \approx [1.3, 2.4]$. Since IonQ has all-to-all connectivity but does not offer parallel gates, the scaling of gate count and depth is $O(n^2)$. The best case would be to achieve fully parallelized gates without increased error per gate, which on IonQ could include gates that share an ion, for a (n) x smaller gate depth. These give a range $b_{\text{depth}} \in [(6/3)^2/6, (6/3)^2] = [0.67, 4]$. Lastly it was previously argued that within the same device crosstalk per gate is independent of n , and also that linear topology crosstalk is independent of n , both of which imply $c_{\text{crosstalk}} = 1$. This calculation suggests that error per gate in IonQ must be reduced by $r \approx [1.3, 2.4] * [0.67, 4] * 1 \approx [0.87, 9.6]$ in order to

reach the Lyapunov regime on six qubits.

This is extrapolated up to 12 qubits in Fig. 6. While IonQ shows more promise overall than IBM-Q, both ranges represent great uncertainty about how future quantum devices will be designed, and current devices are likely closer to the worst case in both.

For IBM-Q one can also estimate the current initial decay rate Γ_0 on six qubits as (current Γ_0 on three qubits) $\cdot b_{\text{depth}} \cdot c_{\text{crosstalk}}$. Current six-qubit clusters have nearly linear topology and IBM-Q’s current gate depth optimization algorithms likely do not find a larger factor of improvement for six qubits than for three, which without parallelization would mean $O(n^3)$ scaling. However good parallelization seems likely, reducing gate depth by up to $(n/2)\times$. Together these suggest $b_{\text{depth}} = (6/3)^3/3$. On linear topology it was argued $c_{\text{crosstalk}} = 1$. This suggests a minimal current Γ_0 on six qubits of $1.4 \cdot 8/3 \cdot 1 \approx 3.7$, shown in Fig. 3.

5 Conclusion

In this paper a signature of semiclassical chaos in a quantum system was studied and minimal bounds were given for its observation in future quantum simulations on few-qubit quantum devices. This signature is the slowing of quantum fidelity decay down to the classical Lyapunov exponent rate when the dynamics are chaotic (diffusive) and noise is large yet not too large.

To find the most plausible route to Lyapunov decay, a particularly resource-efficient quantum map was chosen, the quantum sawtooth map. The classical and quantum dynamics of this map were described, bounds on its dynamical localization were given, and simulations of its time and noise regimes were shown.

Having established the context for this goal, the specifics of the quantum sawtooth map were used to derive three bounds in parameter space that must be satisfied to observe Lyapunov decay. For each a quantitative bound was given, and together those bounds formed a triangular “Lyapunov regime” shown in Fig. 3. From this it was predicted that a minimum of six qubits is necessary to observe Lyapunov decay in the quantum sawtooth map, independent of hardware platform. While other quantum maps were not analyzed closely, they are largely expected to

require at least six qubits and even less noise.

Lastly, numerical simulations and experimental data [37] were employed to chart a path forward, shown in Fig. 6. While the numerical results showed concretely how six or more qubits could exhibit Lyapunov decay, the experimental results were used as a reference point for noise. Rather than attempting to quantify noise sources, recent IBM-Q experiments were assumed to capture the relevant processes and scaling arguments were employed to extrapolate to future experiments. The result was that a minimum of 2.5 – 13x less error per CNOT gate on IBM-Q, including crosstalk, should enable an observation of Lyapunov decay on six qubits. For more qubits the larger Hilbert space lowers the $1/N$ fidelity limit and greatly reduced the difficulty of scaling up. However large uncertainty about the architecture of future superconducting devices produced a large range of error reduction factors. IonQ was estimated to need 0.87 – 9.6x less error per Mølmer-Sørensen gate to observe Lyapunov decay on six qubits. The combination of all-to-all connectivity, low number of neighbors for potential crosstalk, and potential for parallelization gave an advantage over IBM-Q, and allowed for even better scaling to more qubits. However current errors were more approximate than for IBM-Q, so a QSM experiment on three qubits would provide a more precise estimate. While these error reduction requirements are not small, they are for a dynamical signature that is robust to, and even dependent on, large noise. As such they provide an excellent example of how quantum advantage for chaotic dynamical simulations will be an important near term milestone for the field.

While Sec. 4.2 only gave noise reduction requirements for IBM-Q’s superconducting architecture and IonQ’s trapped ion architecture, there are many promising quantum testbeds coming online for which a similar analysis can be performed. Other near term platforms that use superconductors, trapped ions, neutral atoms, or photons may have more favorable trade offs in terms of gate depth, connectivity, crosstalk, and other factors that could help to reach the Lyapunov regime more quickly. One such example is the optimal control approach used by the LLNL Quantum Design and Integration Testbed (QuDIT) [53, 54], which was shown to outperform

Rigetti by over an order of magnitude in simulation depth, in proportion to the length of the native gate decomposition [55]. However the QUDIT platform is currently limited to a single four-level qudit, with plans to scale up.

Out-of-time-ordered correlators (OTOCs) are a quantum analogue to the classical Lyapunov exponent that have been widely explored recently, but were not considered in this work. They allow probing of exponential information scrambling in quantum-chaotic systems. [56, 57] Recent work suggests deep connections between the fidelity (Loschmidt echo) and OTOCs. [58] Both could potentially detect quantum chaos on near-term quantum devices, and OTOCs were even noted recently to show an exponential trend on fewer qubits than the fidelity [59]. However the OTOC growth rate is known to differ in several ways from the Lyapunov exponent [56] so the fidelity may be more reliable for quantum-classical correspondence. Additionally the fidelity is perfectly suited to observing the Lyapunov exponent in the presence of large noise, whereas the study of quantum-classical correspondence of OTOCs in the presence of noise is still developing [60, 61].

In addition to the single-body quantum chaos studied here, simulating many-body quantum chaos is also of great interest. A popular choice for this is quantum spin chains with local interactions, partly due to their natural mapping to qubits with local gates. However quantum maps can also be generalized to many-body systems by adding local coupling terms in the potential energy. One example is the classical many-body kicked rotor [62], which has a corresponding quantum Hamiltonian [17] and therefore a quantum map. This allows simulation of many-body quantum chaos without need for trotterization, potentially realizing interesting dynamics in fewer time steps. The main questions are whether this gain is undone by the need for a quantum Fourier transform and whether efficient algorithms for such systems exist.

The fields of quantum and classical chaos are ripe for exploration via quantum simulation, and hopefully the milestone predicted here will be the first of many similar advances.

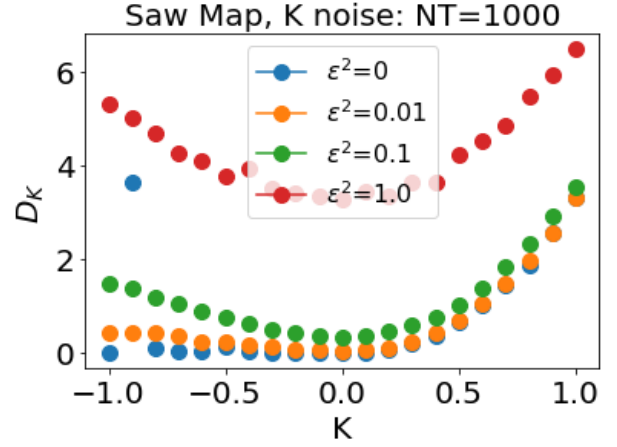


Figure 7: Classical diffusion dependence on the variance ϵ^2 of random noise in parameter K .

Acknowledgements

The authors thank the Quantum Leap group at LLNL for stimulating discussions and ideas that improved the manuscript, including Vasily Geyko, Frank R. Graziani, Stephen B. Libby, Roger W. Minich, and Yuan Shi. In particular we thank Vasily Geyko for performing a comparison of the Rigetti and IBM-Q platforms. We also thank Kristin M. Beck, Alessandro R. Castelli, Jonathan L. DuBois, and Yaniv J. Rosen of the Quantum Coherent Device Physics group at LLNL and Robert Tyler Sutherland at UT San Antonio for their insights into quantum hardware and noise processes. We thank Philippe Jacquod at the University of Geneva for clarifying discussion of the bandwidth limit.

This work was performed by LLNL under the auspices of the U. S. DOE under Contract DE-AC52-07NA27344 and was supported by the DOE Office of Fusion Energy Sciences “Quantum Leap for Fusion Energy Sciences” project FWP-SCW1680 and by LLNL Laboratory Directed Research and Development project 19-FS-078.

A Effect of noise on the classical sawtooth map

Noise in a classical sawtooth map can be understood through its effect on diffusion. For the random noise in parameter K considered in this paper the noise itself can dominate the diffusion, potentially affecting the localization condition in the quantum system. As shown in Fig. 7 the ef-

fect of noise is greatest in the integrable regime $-4 < K < 0$, but still significant in the chaotic regime $K > 0$. When the dynamics are chaotic these results can be understood through a random phase approximation

$$\begin{aligned} D_{K,\epsilon} &\approx \langle (\Delta J)^2 \rangle = \frac{1}{2\pi} \int_{-\pi}^{\pi} d\theta \langle (K + \xi)^2 \rangle \theta^2 \\ &= \frac{\pi^2}{3} (K^2 + \epsilon^2) \end{aligned} \quad (21)$$

Different dependence can occur for different types of noise. For instance noise directly in the update rule for θ has a negligible effect on diffusion in the chaotic regime, as shown for the standard map in Fig. 5.20 of Lichtenberg and Lieberman [63].

Note that one can use $\epsilon = \sigma * 2\pi L/N$ to convert σ to ϵ in the Lyapunov regime, with $L = 1$ assumed to maximize the extent of the Lyapunov regime. For the largest σ at various $n \leq 12$ one finds $\epsilon^2 < 0.01$, suggesting a negligible noise effect on diffusion for $K \gg 0.1$.

References

- [1] Sergio Boixo, Sergei V Isakov, Vadim N Smelyanskiy, Ryan Babbush, Nan Ding, Zhang Jiang, Michael J Bremner, John M Martinis, and Hartmut Neven. Characterizing quantum supremacy in near-term devices. *Nature Physics*, 14(6):595–600, 2018.
- [2] Frank Arute, Kunal Arya, Ryan Babbush, Dave Bacon, Joseph C Bardin, Rami Barends, Rupak Biswas, Sergio Boixo, Fernando GSL Brandao, David A Buell, et al. Quantum supremacy using a programmable superconducting processor. *Nature*, 574(7779):505–510, 2019.
- [3] Ryan Babbush. Google quantum summer symposium 2021: Google’s perspective on the viable applications of early fault-tolerant quantum computers. <https://www.youtube.com/watch?v=-fcQt5C2XGY&list=PLp02pyKis0jL7JdCjzMe0Y1w3TnwTkBT-&index=16>. Accessed: 2021-09-27.
- [4] Richard P. Feynman. *Int. J. Theor. Phys.*, 21:467, 1982.
- [5] Yuri Manin. Computable and uncomputable. *Sovetskoye Radio, Moscow*, 128, 1980.
- [6] Seth Lloyd. *Science*, 273:1073, 1996.
- [7] Giuliano Benenti, Giulio Casati, Simone Montangero, and Dima L Shepelyansky. Efficient quantum computing of complex dynamics. *Physical Review Letters*, 87(22):227901, 2001.
- [8] Giuliano Benenti, Giulio Casati, and Simone Montangero. Quantum computing and information extraction for dynamical quantum systems. *Quantum Information Processing*, 3(1):273–293, 2004.
- [9] Ilon Joseph. Koopman–von neumann approach to quantum simulation of nonlinear classical dynamics. *Physical Review Research*, 2(4):043102, 2020.
- [10] Ilya Y Dodin and Edward A Startsev. On applications of quantum computing to plasma simulations. *arXiv preprint arXiv:2005.14369*, 2020.
- [11] Jin-Peng Liu, Herman Øie Kolden, Hari K Krovi, Nuno F Loureiro, Konstantina Trivisa, and Andrew M Childs. Efficient quantum algorithm for dissipative nonlinear differential equations. *arXiv preprint arXiv:2011.03185*, 2020.
- [12] Seth Lloyd, Giacomo De Palma, Can Gokler, Bobak Kiani, Zi-Wen Liu, Milad Marvian, Felix Tennie, and Tim Palmer. Quantum algorithm for nonlinear differential equations. *arXiv preprint arXiv:2011.06571*, 2020.
- [13] Alexander Engel, Graeme Smith, and Scott E Parker. Linear embedding of nonlinear dynamical systems and prospects for efficient quantum algorithms. *Physics of Plasmas*, 28(6):062305, 2021.
- [14] IY Dodin and EA Startsev. Quantum computation of nonlinear maps. *arXiv preprint arXiv:2105.07317*, 2021.
- [15] Aram W Harrow, Avinandan Hassidim, and Seth Lloyd. Quantum algorithm for linear systems of equations. *Physical Review Letters*, 103(15):150502, 2009.
- [16] Andrew M Childs, Robin Kothari, and Rolando D Somma. Quantum algorithm for systems of linear equations with exponentially improved dependence on precision. *SIAM Journal on Computing*, 46(6):1920–1950, 2017.

- [17] Simone Notarnicola, Alessandro Silva, Rosario Fazio, and Angelo Russomanno. Slow heating in a quantum coupled kicked rotors system. *Journal of Statistical Mechanics: Theory and Experiment*, 2020(2):024008, 2020.
- [18] Bertrand Georgeot and Dima L Shepelyansky. Exponential gain in quantum computing of quantum chaos and localization. *Physical Review Letters*, 86(13):2890, 2001.
- [19] Benjamin Lévi and Bertrand Georgeot. Quantum computation of a complex system: The kicked harper model. *Physical Review E*, 70(5):056218, 2004.
- [20] Klaus M Frahm, Robert Fleckinger, and Dima L Shepelyansky. Quantum chaos and random matrix theory for fidelity decay in quantum computations with static imperfections. *The European Physical Journal D-Atomic, Molecular, Optical and Plasma Physics*, 29(1):139–155, 2004.
- [21] Rüdiger Schack. Using a quantum computer to investigate quantum chaos. *Physical Review A*, 57(3):1634, 1998.
- [22] Giuliano Benenti and Giulio Casati. Quantum-classical correspondence in perturbed chaotic systems. *Physical Review E*, 65(6):066205, 2002.
- [23] Giuliano Benenti, Giulio Casati, Simone Montangero, and Dima L Shepelyansky. Dynamical localization simulated on a few-qubit quantum computer. *Physical Review A*, 67(5):052312, 2003.
- [24] Wen-ge Wang, Giulio Casati, and Baowen Li. Stability of quantum motion: Beyond fermi-golden-rule and lyapunov decay. *Physical Review E*, 69(2):025201, 2004.
- [25] Philippe Jacquod and Cyril Petitjean. Decoherence, entanglement and irreversibility in quantum dynamical systems with few degrees of freedom. *Advances in Physics*, 58(2):67–196, 2009.
- [26] Thomas Gorin, Tomaž Prosen, Thomas H Seligman, and Marko Žnidarič. Dynamics of loschmidt echoes and fidelity decay. *Physics Reports*, 435(2-5):33–156, 2006.
- [27] Arseni Goussev, Rodolfo A Jalabert, Horacio M Pastawski, and Diego Wisniacki. Loschmidt echo. *arXiv preprint arXiv:1206.6348*, 2012.
- [28] Bruno Eckhardt. Echoes in classical dynamical systems. *Journal of Physics A: Mathematical and General*, 36(2):371, 2002.
- [29] Asher Peres. Stability of quantum motion in chaotic and regular systems. *Physical Review A*, 30(4):1610, 1984.
- [30] Rodolfo A Jalabert and Horacio M Pastawski. Environment-independent decoherence rate in classically chaotic systems. *Physical Review Letters*, 86(12):2490, 2001.
- [31] Philippe Jacquod, Peter G Silvestrov, and Carlo WJ Beenakker. Golden rule decay versus lyapunov decay of the quantum loschmidt echo. *Physical Review E*, 64(5):055203, 2001.
- [32] Natalia Ares and Diego A Wisniacki. Loschmidt echo and the local density of states. *Physical Review E*, 80(4):046216, 2009.
- [33] Ignacio García-Mata and Diego A Wisniacki. Loschmidt echo in quantum maps: the elusive nature of the lyapunov regime. *Journal of Physics A: Mathematical and Theoretical*, 44(31):315101, 2011.
- [34] Robert Tyler Sutherland. Private communication, July 2021.
- [35] Mohit Pandey, Pieter W Claeys, David K Campbell, Anatoli Polkovnikov, and Dries Sels. Adiabatic eigenstate deformations as a sensitive probe for quantum chaos. *Physical Review X*, 10(4):041017, 2020.
- [36] Pedram Roushan et al. Spectroscopic signatures of localization with interacting photons in superconducting qubits. *Science*, 358(6367):1175–1179, 2017.
- [37] Max D Porter and Ilon Joseph. Manuscript in preparation.
- [38] A Lakshminarayan and NL Balazs. On the quantum cat and sawtooth maps—return to generic behaviour. *Chaos, Solitons & Fractals*, 5(7):1169–1179, 1995.
- [39] David J Griffiths. *Introduction to Quantum Mechanics*, page 116. Pearson Prentice Hall, second edition, 2005.

- [40] Fausto Borgonovi. Localization in discontinuous quantum systems. *Physical Review Letters*, 80(21):4653, 1998.
- [41] Giulio Casati and Tomaž Prosen. Quantum localization and cantori in the stadium billiard. *Physical Review E*, 59(3):R2516, 1999.
- [42] RE Prange, R Narevich, and Oleg Zaitsev. Quasiclassical surface of section perturbation theory. *Physical Review E*, 59(2):1694, 1999.
- [43] Fernando M Cucchietti, Horacio M Pastawski, and Rodolfo A Jalabert. Universality of the lyapunov regime for the loschmidt echo. *Physical Review B*, 70(3):035311, 2004.
- [44] Fernando M Cucchietti. The loschmidt echo in classically chaotic systems: Quantum chaos, irreversibility and decoherence. *arXiv preprint quant-ph/0410121*, 2004.
- [45] Thanos Manos and Marko Robnik. Dynamical localization in chaotic systems: Spectral statistics and localization measure in the kicked rotator as a paradigm for time-dependent and time-independent systems. *Physical Review E*, 87(6):062905, 2013.
- [46] Tanay Roy, Sumeru Hazra, Suman Kundu, Madhavi Chand, Meghan P Patankar, and R Vijay. A programmable three-qubit superconducting processor with all-to-all connectivity. *arXiv preprint arXiv:1809.00668*, 2018.
- [47] Brian Marinelli, Jie Luo, Kyunghoon Lee, David Santiago, and Irfan Siddiqi. A dynamically reconfigurable quantum processor architecture. *Bulletin of the American Physical Society*, 2021.
- [48] Doug McClure. Quantum computing stack exchange answer. <https://quantumcomputing.stackexchange.com/questions/9073/what-does-the-error-rate-on-the-ibmq-website-mean>. Accessed: 2021-09-17.
- [49] Dmitri Maslov. Basic circuit compilation techniques for an ion-trap quantum machine. *New Journal of Physics*, 19(2):023035, 2017.
- [50] Kenneth Wright, Kristin M Beck, et al. Benchmarking an 11-qubit quantum computer. *Nature Communications*, 10(1):1–6, 2019.
- [51] Nikodem Grzesiak et al. Efficient arbitrary simultaneously entangling gates on a trapped-ion quantum computer. *Nature Communications*, 11(1):1–6, 2020.
- [52] David Kielpinski, Chris Monroe, and David J Wineland. Architecture for a large-scale ion-trap quantum computer. *Nature*, 417(6890):709–711, 2002.
- [53] Xian Wu, Spencer L Tomarken, N Anders Petersson, Luis A Martinez, Yaniv J Rosen, and Jonathan L DuBois. High-fidelity software-defined quantum logic on a superconducting qudit. *Physical Review Letters*, 125(17):170502, 2020.
- [54] Eric T Holland, Kyle A Wendt, Konstantinos Kravvaris, Xian Wu, W Erich Ormand, Jonathan L DuBois, Sofia Quaglioni, and Francesco Pederiva. Optimal control for the quantum simulation of nuclear dynamics. *Physical Review A*, 101(6):062307, 2020.
- [55] Yuan Shi, Alessandro R Castelli, Ilon Joseph, Vasily Geyko, Frank R Graziani, Stephen B Libby, Jeffrey B Parker, Yaniv J Rosen, and Jonathan L DuBois. Quantum computation of three-wave interactions with engineered cubic couplings.
- [56] Efim B Rozenbaum, Sriram Ganeshan, and Victor Galitski. Lyapunov exponent and out-of-time-ordered correlator’s growth rate in a chaotic system. *Physical Review Letters*, 118(8):086801, 2017.
- [57] AI Larkin and Yu N Ovchinnikov. Quasi-classical method in the theory of superconductivity. *Sov Phys JETP*, 28(6):1200–1205, 1969.
- [58] Bin Yan, Lukasz Cincio, and Wojciech H Zurek. Information scrambling and loschmidt echo. *Physical Review Letters*, 124(16):160603, 2020.
- [59] Sreeram PG, Vaibhav Madhok, and Arul Lakshminarayan. Out-of-time-ordered correlators and the loschmidt echo in the quantum kicked top: how low can we go? *Journal of Physics D: Applied Physics*, 54(27):274004, 2021.

- [60] Jorge Chávez-Carlos, B López-del Carpio, Miguel A Bastarrachea-Magnani, Pavel Stránský, Sergio Lerma-Hernández, Lea F Santos, and Jorge G Hirsch. Quantum and classical lyapunov exponents in atom-field interaction systems. *Physical Review Letters*, 122(2):024101, 2019.
- [61] Tomer Goldfriend and Jorge Kurchan. Quasi-integrable systems are slow to thermalize but may be good scramblers. *Physical Review E*, 102(2):022201, 2020.
- [62] Atanu Rajak, Roberta Citro, and Emanuele G Dalla Torre. Stability and pre-thermalization in chains of classical kicked rotors. *Journal of Physics A: Mathematical and Theoretical*, 51(46):465001, 2018.
- [63] Allan J Lichtenberg and Michael A Lieberman. *Regular and chaotic dynamics*, volume 38. Springer Science & Business Media, 1992.